

Electrically Controlled Adsorption of Oxygen in Bilayer Graphene Devices

Yoshiaki Sato,^{1,*} Kazuyuki Takai,¹ and Toshiaki Enoki¹

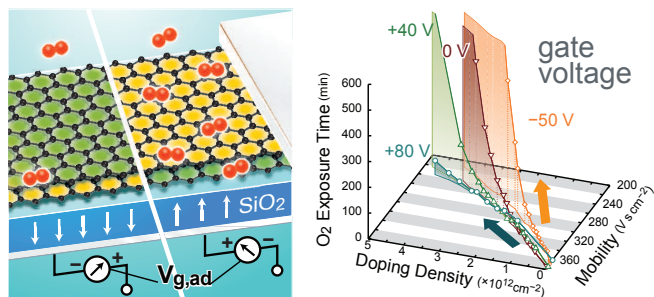
¹*Department of Chemistry, Tokyo Institute of Technology, 2-12-1 Ookayama, Meguro-ku, Tokyo, 152-8551, Japan*

We investigate the chemisorptions of oxygen molecules on bilayer graphene (BLG) and its electrically modified charge-doping effect using conductivity measurement of the field effect transistor channeled with BLG. We demonstrate that the change of the Fermi level by manipulating the gate electric field significantly affects not only the rate of molecular adsorption but also the carrier-scattering strength of adsorbed molecules. Exploration of the charge transfer kinetics reveals the electrochemical nature of the oxygen adsorption on BLG. [This document is the unedited Author's version of a Submitted Work that was subsequently accepted for publication in *Nano Letters*, ©American Chemical Society after peer review. To access the final edited and published work see <http://dx.doi.org/10.1021/nl202002p>.]

Keywords: Graphene; charge transfer; field effect transistor; electron transport; mobility; band gap

It has been a central topic of surface science how to control the adsorption and desorption in order to bring out desirable features and functionalities by adsorbed molecules. Tuning the electronic features of solid surfaces has an important implication in that molecular chemisorptions and catalytic reactions are determined by them^{1,2}. In particular for graphene, the two-dimensional honeycomb carbon lattice, in which the conduction π^* -band and the valence π -band contact to each other at the “Dirac point” giving a feature of zero-gap semiconductor³, the control of chemisorption is a critical issue since chemisorption directly leads to altering every electronic property of graphene. Other than the electron/hole doping⁴ owing to the charge transfer between graphene and the adsorbed molecules, widely known are the charged impurity effect on the electron transport^{5–7}, lattice deformation⁸, and opening the band gap due to asymmetric adsorption^{9–11}. Aside from the macroscopic spatially-controlled adsorption that is achieved using nano-device fabrication technique¹², microscopic control of adsorption structure is of great importance because the aforementioned adsorption effects are altered by the local structure of adsorbate, e.g., whether the adsorbed molecules are arranged in a random or superlattice structure^{10,13}, or whether the molecules are adsorbed individually^{4,14} or collectively (in dimers¹⁵ or clusters^{16,17}). For the first step to realize such an advanced control of adsorption, the methods to utilize the interaction between the adsorbed molecules and graphene for it are to be explored.

The principal impetus in the present study is to control the charge transfer between graphene and the adsorbed molecules by tuning the Fermi level of graphene, which is readily accomplished in the field effect transistor (FET) structure. When SiO_2/Si substrate is used as the back-gate insulator of the FET, the tuning range of the Fermi level of graphene by the application of the gate voltage is at the extent of several ± 0.1 eV¹⁸ which would be sufficient to alter the chemical reactivity on the surface. Besides, the additional charge and the gradient of electric potential generated by the gate electric



field are expected to change the polarization of adsorbed molecules^{19,20} and to modify the charge distribution on graphene layers and the adsorbed molecules^{21–25} leading to, e.g., the change in the ease of migration of molecules adsorbed on graphene²⁶. Some research^{27–29} argues that the change in the Fermi level caused by a gate electric field activates electrochemical redox reactions and the accompanying charge transfer causes hysteresis of the source–drain current in graphene FET, yet there has been no investigation that elucidates the relation between the kinetics of adsorption to graphene and gate electric field. In this study we investigated gate-tuned molecular oxygen adsorption through systematic measurements of conductivity using mainly bilayer graphene (BLG).

The back-gated BLG-FETs were fabricated on SiO_2 (300 nm thick) on heavily n-doped silicon substrate by means of photolithography. The channel length and width were 6 μm and 3.5 μm , respectively. Prior to measurement, we repeated vacuum annealing (210°C, 10 h) to remove the adsorbed moisture and contaminants on the surface until no more changes in the gate-dependent conductivity σ were eventually seen. After the annealing, the BLG-FET exhibited its pristine nature, that is, ambipolar transport properties with a conductivity minimum around $V_g = V_{\text{CNP}}^0 < 8$ V giving the “charge neutrality point (CNP)” with electrons and holes in BLG being equal in density. The Drude mobility $\mu(n)$ was estimated to be $\sim 1 \times 10^3$ $\text{cm}^2\text{V}^{-1}\text{s}^{-1}$ from the equation $\mu(n) = \sigma/e|n|$, where n is the carrier density with $n = (c_g/e)(V_g - V_{\text{CNP}})$ ($c_g/e = 7 \times 10^{10}$ $\text{cm}^{-2}\text{V}^{-1}$;

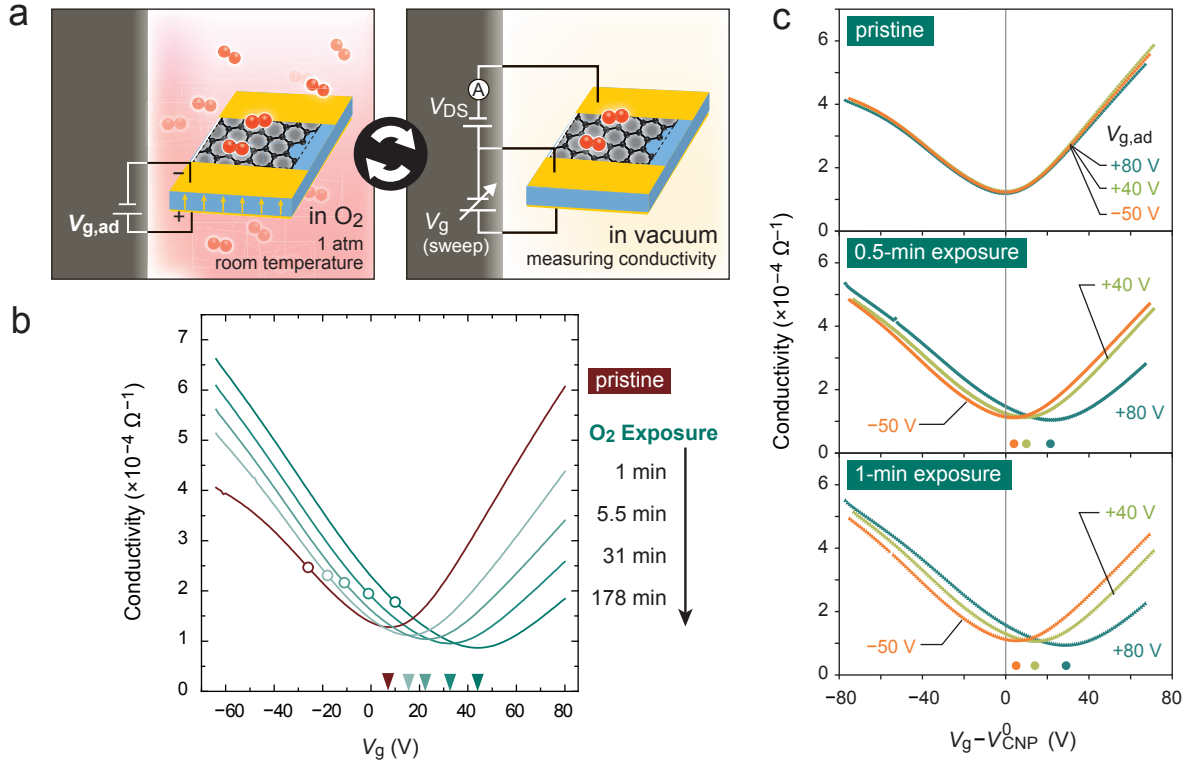


FIG. 1: (a) Schematic of the measurement cycle. First, the field effect transistor channeled by bilayer graphene (BLG-FET) is exposed to gaseous O_2 while the gate voltage $V_{g,ad}$ is applied (left panel). Then the system is evacuated and the source-drain conductivity of the BLG-FET is measured by sweeping the gate voltage V_g (right panel). Subsequently gaseous O_2 is again introduced, and the cycle is repeated. The gas introduction and evacuation are completed in a shorter time than ~ 10 s to prevent additional gas from adsorption. The whole cycle is executed at room temperature. (b) Change of the field effect behavior due to the O_2 exposure with $V_{g,ad} = 0$ V (run 1). The gate voltage giving the minimum conductivity (the charge neutrality point), is shifted from $V_g = V_{CNP}^0$ (< 8 V) (marked by a brown triangle, before O_2 exposure) to the positive direction (green triangles) upon O_2 exposure. Circles on the curves represent the conductivity at the hole density of $2.5 \times 10^{12} \text{ cm}^{-2}$ that are used to calculate Drude conductivity shown in Figure 4a. (c) The same measurement as in the panel (b) with applying the finite $V_{g,ad}$. All the curves are shifted by $-V_{CNP}^0$ ($V_{CNP}^0 = 13, 9,$ and 11 V for the run of $V_{g,ad} = +80, +40,$ and -50 V, respectively) in V_g direction, i.e., the charge neutrality points of the pristine graphene without the adsorbed oxygen are taken as zero gate voltage. The top panel of (c) represents the σ vs $V_g - V_{CNP}^0$ for the pristine graphene. The changes of σ vs $V_g - V_{CNP}^0$ curve after a single and a double exposure to O_2 (the time duration of a single exposure is 30 s) are shown in the center and the lower panel of (c), respectively. Filled circles indicate $V_{shift} = V_{CNP} - V_{CNP}^0$ (the shift of the CNP) for each curve.

c_g is the capacitance per unit area for the back-gated graphene FET on 300 nm-thick SiO_2)²². It is in the range of the values for BLG-FET in two-probe configuration previously reported⁶, and therefore we confirm that the graphene of the present BLG-FET has few defects that may extremely enhance the chemical reactivity of graphene³⁰.

Next we exposed the BLG-FET to 1 atm of high-purity ($>99.9995\%$) oxygen in the measurement chamber at room temperature. Instead of measuring conductivity with graphene kept in the O_2 environment, we performed the short-time interval exposure-evacuation cycles schematically shown in Figure 1a; O_2 exposure was done under the dc gate voltage $V_{g,ad}$, followed by rapid evacuation in less than 10 s (the physisorbed O_2 molecules would be removed immediately without charge transfer), and eventually the σ vs V_g measurement was

done with sweeping V_g under vacuum. In this cycle, we can rule out the possibility of the additional oxygen adsorption during sweeping gate voltage for the σ vs V_g measurement since the system was evacuated then. In addition, we found that the σ vs V_g curve did not vary under vacuum at room temperature at least for more than several hours, so that we can also rule out the possibility of the oxygen desorption during σ vs V_g measurement (taking ca. 10 min to obtain a single σ vs V_g curve). Therefore, just repeating the cycles substantially realizes the long-time O_2 exposure under $V_{g,ad}$, the length of which is denoted by total O_2 exposure time, t . Figure 1b shows the change in σ vs V_g by repeating the O_2 exposure-evacuation cycles without applying gate voltage during O_2 exposure (run 1, $V_{g,ad} = 0$ V). The shift of the charge neutrality point by the amount of $V_{shift}(t) = V_{CNP}(t) - V_{CNP}^0$ toward the positive di-

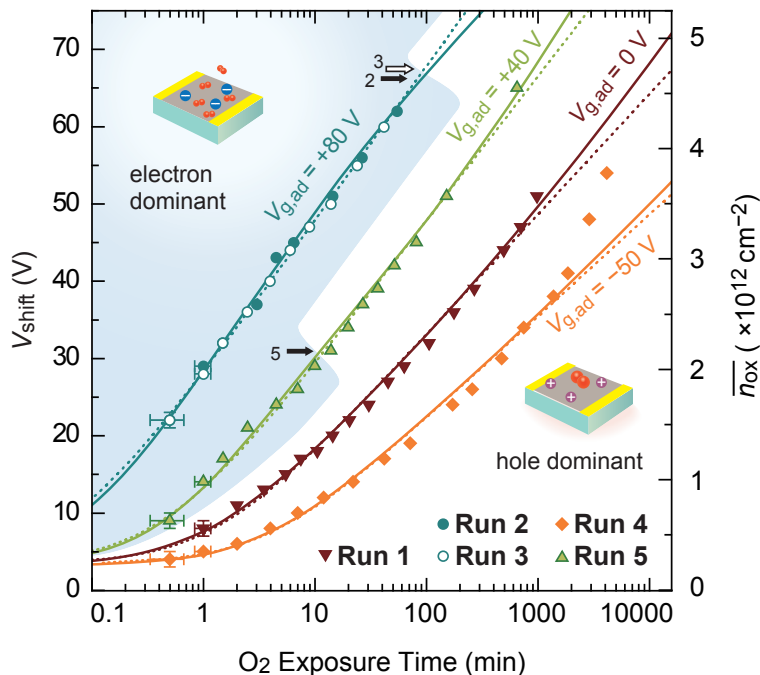


FIG. 2: Time dependence of V_{shift} and doping density \bar{n}_{ox} with doping due to the O_2 exposure under application of various $V_{\text{g,ad}}$. Solid and dotted curves are the fits based on the H kinetics and the P kinetics (see text), respectively. The curve fitting is made in the range of exposure time below 2000 min. The electron-dominant region, where the Fermi level of BLG is higher than the CNP ($V_{\text{g,ad}} > V_{\text{CNP}}$), is painted blue and the hole-dominant region ($V_{\text{g,ad}} < V_{\text{CNP}}$) is painted white. Carrier type is inverted between electron and hole at the point indicated by arrows (numbers aside correspond to the run number) during the evolution of the oxygen adsorption.

rection was observed (Figure 1b), which represents hole doping to graphene. Prolonged exposure brought further hole doping, and eventually the doping density (induced charge by the oxygen adsorption) $\bar{n}_{\text{ox}}(t) = (c_{\text{g}}/e)V_{\text{shift}}(t)$ reached more than $5 \times 10^{12} \text{ cm}^{-2}$ within a time scale of 10^3 min. Note that any hysteresis as observed in graphene FET in moist atmosphere^{29,31–34} was not found in the observed σ vs V_{g} curve, so that we can uniquely determine $V_{\text{CNP}}(t)$ as a function of t . Another remarkable feature is the hole conductivity in highly doped regime, $V_{\text{g}} - V_{\text{CNP}}(t) < -40$ V (i.e., $|n| > 3 \times 10^{12} \text{ cm}^{-2}$). The σ vs V_{g} curve distorted and exhibited the sublinear dependence in this regime for the pristine BLG-FET as can be seen in Figure 1b. Yet it disappeared only after the exposure to O_2 for 1 min, whereas the carrier doping has not proceeded much at that time. Thus this rapid change in conductivity feature is discriminated from the slower change causing the shift of the CNP; one possibility is that the former is due to rapid oxidation of the metal-graphene interface^{35,36}, which does not shift the Fermi level of graphene but asymmetrically varies the conductivity.

Both V_{CNP} and the mobility of the BLG-FET with the oxygen adsorbed were reset to the value for the pristine BLG-FET by annealing the O_2 -exposed BLG-FET in vacuum at 200°C , indicating that O_2 desorption readily proceeds at high temperature without making any defects. By virtue of this reversibility of the oxygen ad-

sorption, we can repeat the conductivity measurements in the exposure–evacuation cycles as described above for the same device and compare the results. We additionally carried out four consecutive measurements under the same condition except that a finite gate voltage $V_{\text{g,ad}}$ was applied during O_2 exposure; $V_{\text{g,ad}}$ was $+80$ V (run 2 and run 3), -50 V (run 4) and $+40$ V (run 5). Figure 1c represents the change of the gate-dependent conductivity σ vs $V_{\text{g}} - V_{\text{CNP}}^0$ at the initial step of the runs 2, 4, 5: before O_2 exposure, (i.e., after vacuum annealing) and after the first and second exposure–evacuation cycles (the duration time for O_2 exposure in each cycle is 30 s, i.e., $t = 0.5, 1$ min, after the first and second cycle, respectively). All the σ vs $V_{\text{g}} - V_{\text{CNP}}^0$ curves collapsed onto almost the identical curve in the pristine graphene as shown in the top panel of Figure 1c. Since V_{CNP}^0 was within 10 ± 3 V for each run (see the caption of Figure 1), the BLG-FET was realized to exhibit its pristine feature before O_2 exposure. After the O_2 exposure (the center and the bottom panel of Figure 1c) the gate-dependent conductivity changes similarly as was also observed for run 1 (Figure 1b), but the effect of applying $V_{\text{g,ad}}$ during O_2 exposure is marked by the clear difference in $V_{\text{shift}}(t)$. There is a tendency that $V_{\text{shift}}(t)$ is larger for higher $V_{\text{g,ad}}$ and smaller for lower $V_{\text{g,ad}}$, indicating that hole doping proceeds more intensively to graphene with higher Fermi level. This trend is pronounced on the increase in the exposure time, as confirmed by comparing the center and

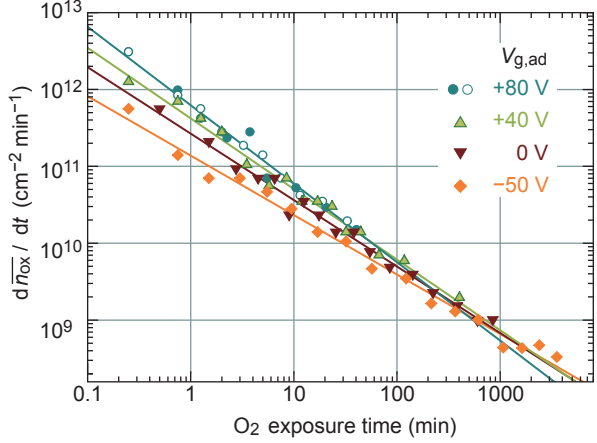


FIG. 3: Double logarithmic plot of time dependence of $d\bar{n}_{ox}/dt$. Symbols are taken in common with Figure 2. We estimate $d\bar{n}_{ox}/dt$ from the differential between the neighboring data points for each run in Figure 2. Lines are linear fits for all the differential data. The slope of each curve gives $u = 1.02, 0.91, 0.86,$ and 0.77 ($d\bar{n}_{ox}/dt \propto t^{-u}$) for the gate voltage $V_{g,ad} = +80, +40, 0,$ and -50 V, respectively.

the bottom panel of Figure 1(c).

We tracked the temporal evolution of the gate-dependent conductivity over a wide time range between 10^0 – 10^3 min. Figure 2 represents V_{shift} for runs 1–5 with respect to O_2 exposure time, in which the corresponding doping density owing to the oxygen adsorption, \bar{n}_{ox} , is also shown in the right axis. The tendency that the high $V_{g,ad}$ leads to rapid doping can be seen clearly over a whole time range; e.g., to reach the doping level of $V_{\text{shift}} = 40$ V, it took ca. 300 min for nonbiased BLG-FET. In contrast, hole doping is so enhanced for the BLG-FET of $V_{g,ad} = 80$ V that it took only 4 min, on the other hand so suppressed for that of $V_{g,ad} = -50$ V that it took more than 1000 min. The doping density increases almost linearly with respect to $\log t$ for $V_{g,ad} = +80$ V and $+40$ V, whereas superlinearly for $V_{g,ad} = 0$ V and -50 V. The plots for runs 2 and 3, having common $V_{g,ad} = +80$ V, are completely on the same line, which verifies that the thermal annealing in vacuum for the reproducing of the undoped state in the BLG does not affect the behavior of adsorption.

Figure 3 shows the time dependence of the doping rate $d\bar{n}_{ox}/dt$ estimated from the differential between the neighboring data points in Figure 2. It is obvious that the doping rate changes in accordance with $d\bar{n}_{ox}/dt \propto t^{-u}$. The power u is dependent on $V_{g,ad}$; $u \approx 1$ for $V_{g,ad} = +80$ V and it decreases for the runs with lower $V_{g,ad}$. This deviates from the conventional Langmuirian kinetics for molecular adsorption which would give $d\bar{n}_{ox}/dt \propto \exp(-t/\tau)$ with a constant τ .

Careful verification is necessary to inquire the gate-voltage-dependent and non-Langmuirian temporal change

of the molecular doping since the rate for doping density $d\bar{n}_{ox}/dt$ is related to both of the rate for the chemisorption of molecules (dN_{ox}/dt , where N_{ox} is the areal density of the adsorbed oxygen molecules) and the transferred charge per adsorbed molecule (the charge/molecular ratio, Z). Therefore, we analyze the mobility that includes the information of the scattering mechanism of the conducting electrons and the charge of the adsorbed molecules. Within a standard Boltzmann approach³⁷, the mobility is changed inversely proportional to the density of the scattering centers (i.e., the adsorbed molecules), N_{ox} . In the realistic case, the inverse mobility is given as a function of N_{ox} and the carrier density n , which reads⁵

$$\frac{1}{\mu(n, N_{ox})} = \frac{N_{ox}}{C(n)} + \frac{1}{\mu_0(n)} \quad (1)$$

Here $\mu_0(n)$ represents the mobility of the pristine graphene without the adsorbed oxygen. The coefficient $C(n)$ represents the feature of carrier scattering by the adsorbed oxygen. On the one hand, the charged-impurity scattering³⁸ gives $C(n) \propto [1 + 6.53\sqrt{n}(d + \lambda_{TF})]/Z^2$ for the BLG in the low-carrier-density regime and in the limit of $d \rightarrow 0$ within the Thomas–Fermi approximation³⁸, where d is the distance between the impurities and the center of the two layers of the BLG (see the inset of Figure 4a for the definition), and the screening length $\lambda_{TF} = \kappa\hbar^2/4m^*e \approx 1$ nm (κ : dielectric constant)³⁸. On the other hand, the short-range delta-correlated scatterers give the constant $C(n) \equiv C_s$ ³⁸, or the strong impurities with the potential radius R give $C(n) \propto [\ln(R\sqrt{\pi n})]^2$ in the off-resonance condition³⁹, which is a decreasing function of n in the regime of $n \sim 10^{12}$ cm^{-2} taking R to be several angstroms. As for the relation between the concentration of the adsorbed oxygen molecules N_{ox} and the O_2 -induced doping density \bar{n}_{ox} , we assume that the charge Ze of each adsorbed oxygen molecule dopes the carriers $-Ze$ in the BLG, notably, $\bar{n}_{ox} = -ZN_{ox}$. To be exact, the amount of the induced charge is not such a simple function⁶ proportional to the number of adsorbed molecules due to the energy-dependent DOS of BLG^{40,41} and the anomalous screening effect therein^{5,6,42}. Yet in the low energy regime of BLG where the DOS is envisaged to be constant, the assumption above is appropriate.

Figure 4a shows the inverse Drude mobility μ^{-1} vs \bar{n}_{ox} plots at the carrier density of $n = 2.5 \times 10^{12}$ cm^{-2} (marked by the open circles in Figure 1b for run 1: $V_{g,ad} = 0$ V) for $V_{g,ad} = +80, +40, 0,$ and -50 V. Linear increase in μ^{-1} with respect to \bar{n}_{ox} was found. This, along with the linearity between μ^{-1} and N_{ox} given by Eq. (1), implies that Z is not a function of N_{ox} , i.e., invariant against the increase of the adsorbed molecules. Interestingly, the slope of μ^{-1} vs \bar{n}_{ox} plot (the *inverse* of the slope corresponds to $C(n)|Z|$ in Eq. (1)) depends on $V_{g,ad}$. Note that before O_2 was introduced ($\bar{n}_{ox} = 0$), we observed $\mu^{-1} \approx 28$ V s m^{-2} irrespective of $V_{g,ad}$, and thus the difference in the mobility by $V_{g,ad}$ genuinely results from

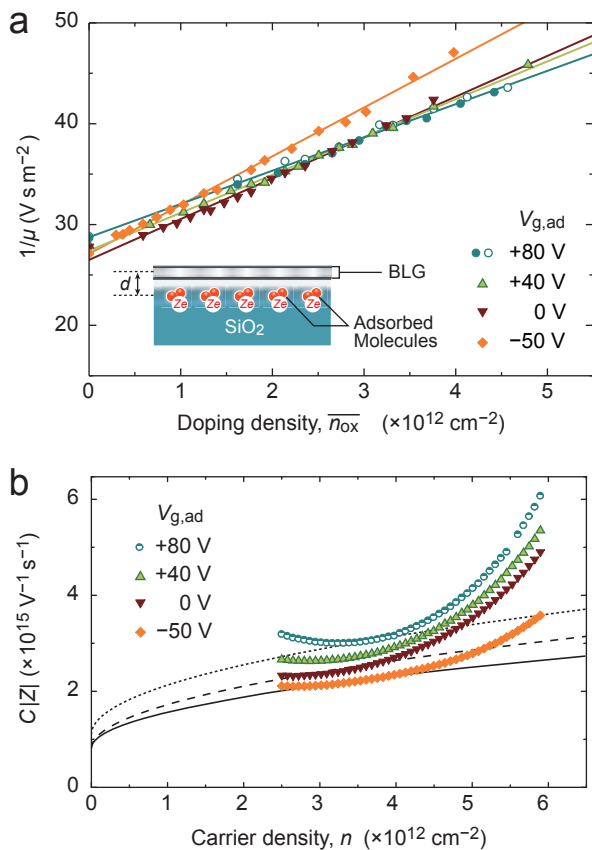


FIG. 4: (a) Inverse mobility μ^{-1} vs the doping density \bar{n}_{ox} for each run in Figure 2. Symbols are taken in common with Figure 2. Lines are linear fits (as for $V_{g,\text{ad}} = +80$ V, the data for both run 2 and run 3 are included). Inset: Adsorbed oxygen species with charge Ze positioned at the distance d away from the center of BLG. (b) $C|Z|$ vs the carrier density n (see Eq. (1)). For $V_{g,\text{ad}} = +80$ V, $C|Z|$ is acquired by gathering the data for run 2 and run 3. Theoretical results based on a charged-impurity scattering mechanism are shown with the various distance d and charge/molecular ratio Z : the solid line represents the result for $d = 0.43$ nm and $Z = 0.38$, the dashed line for $d = 0.73$ nm and $Z = 0.38$, and the dotted line for $d = 0.43$ nm and $Z = 0.28$, respectively.

the adsorbed oxygen instead of other unintentional impurities on the BLG or the SiO_2 substrate. In Figure 4b, the inverse of the slope, $C(n)|Z|$, is shown for the various carrier densities, n . Therein we omit the data in the low carrier regime of $n < 2.5 \times 10^{12} \text{ cm}^{-2}$, in which the residual carriers due to electron-hole puddles cannot be disregarded and the carrier density n (and thus also the Drude mobility) cannot be correctly estimated only by considering the gate electric field effect⁴³. Similarly to the charged impurity model rather than otherwise, $C(n)|Z|$ is increasing with n . The dependence experimentally observed, however, still deviates from the theoretical calculated results within the charged impurity model plotted in Figure 4b for various d and Z (assuming d and Z are invariant to n).

The difference in $C(n)|Z|$ depending upon $V_{g,\text{ad}}$ indicates that the electronic polarity of graphene varies the adsorption states of oxygen molecules, leading to the variation of d and Z . When the positive (negative) $V_{g,\text{ad}}$ is applied, negative (positive) carrier is electrically induced on graphene, which may modify the interaction between graphene and the adsorbed oxygen molecules with the negative charge, e.g., the Coulomb interaction and the overlap of the orbitals. Eventually, the stable adsorption state is varied by $V_{g,\text{ad}}$, leading to the difference in mobility. Besides, let us recall that conductivity measurement process is set apart from the O_2 adsorption process and that constant $V_{g,\text{ad}}$ is not applied when the mobility is measured (Figure 1a). Accordingly, whereas the stable adsorption state of oxygen during the conductivity measurement may differ from that during adsorption, the adsorbed oxygen molecules are kept in the former state during conductivity measurement, and the mobility varying by $V_{g,\text{ad}}$ is actually observed. This indicates that the energetic barrier exists for charge redistribution between graphene and the adsorbed oxygen molecules (shown below), and once the adsorption is accomplished, the charge Ze on each adsorbed oxygen molecules will not immediately change just after switching on/off the gate voltage. One possible reason for the deviation between the experimental results and theoretical curve is that d varies accompanied with the change in n (or sweeping V_g). Yet actually, since modifying d by several angstroms results in the small change in $(C(n)|Z|)$ as shown in Figure 4b, it is necessary to investigate more about the behavior of the adsorbed oxygen molecules in the gate electric field in a the future study.

It is controversial what kind of oxygen species does actually cause the hole doping to graphene. Because the electron affinity of O_2 (0.44 eV⁴⁴) is much lower than the work function of graphene (4.6 eV⁴⁵), direct charge transfer between them seems unfavorable. Instead, with an analogy of the charge doping of diamond surface⁴⁶, there is a widely accepted^{28,33,47} hypothesis that the hole doping proceeds through an electrochemical reaction⁴⁶ such as: $\text{O}_2 + 2\text{H}_2\text{O} + 4e^- = 4\text{OH}^-$, by which the charge transfer is favorable due to the lowered free energy change $\Delta G = -0.7 \text{ eV}^{28}$ on the condition that the oxygen pressure is 1 atm and $\text{pH} = 7$. This electrochemical reaction needs the aid of water that is mostly eliminated in the experiment by annealing (we observed no hysteresis in the σ vs V_g curve, that is, there are few charge traps often attributed to residual moisture on graphene or its substrate). Yet as for graphene deposited on the hydrophilic SiO_2 substrate³², it is possible that a small amount of residual water molecules (more than the chemical equivalent of O_2) are trapped on SiO_2 surface or voids, which cannot be easily removed by the vacuum annealing at 200 °C in comparison with those on graphene surface. We suggest that the electrochemical mechanism is plausible also in our case, yet the adsorbed molecule could be other chemical species than OH^- , the charge of which may be dependent on $V_{g,\text{ad}}$.

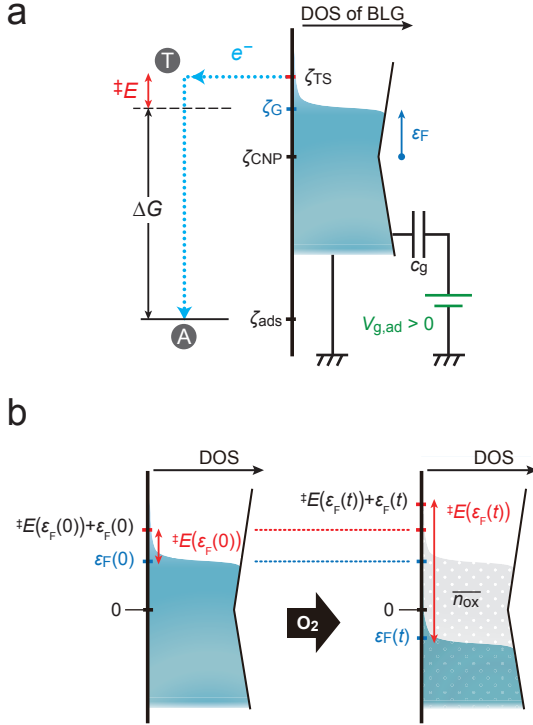


FIG. 5: Schematic energy diagrams of the kinetics of O_2 adsorption (H kinetics). (a) Path for electron transfer in this model is shown by the blue dotted arrow; electrons in BLG (the electrochemical potential ζ_G) are transferred to O_2 molecules via the transition state (the circled T at the level of ζ_{TS}), giving the adsorbed oxygen species (the circled A at the level of ζ_{ads}). The activation energy, the free energy change, and the level of the CNP are denoted by $\ddagger E$, ΔG and ζ_{CNP} , respectively. The Fermi level is defined by $\varepsilon_F = \zeta_G - \zeta_{CNP}$. As a demonstration, the case for $V_{g,ad} > 0$ is presented. (b) Temporal change in the activation energy and the Fermi energy due to the adsorption of oxygen molecules to BLG negatively doped by the positive gate voltage (as in case of panel a). The left panel represents the case before oxygen adsorption ($t = 0$), and the right panel represents the oxygen exposure for the time t . Here the energy is measured from the CNP. The red and the blue tick marks denote the level for the transition state and the Fermi level, respectively. Oxygen adsorption lowers the Fermi level, accompanied with the increase in hole doping of \bar{n}_{ox} (equal to the area of grayed part, $\int_{\varepsilon_F(t)}^{\varepsilon_F(0)} D(\varepsilon_F) d\varepsilon_F$), and the activation energy increases according to Eq. (2)

In light of the discussion above, the electrochemical description^{33,48} is expected to be applicable for the observed adsorption kinetics of oxygen to the BLG. Here we premise that the molecular adsorption is determined by the electrochemical potential of graphene, and consider the charge transfer kinetics in an approach based on Butler–Volmer theory^{49,50}. The model is schematically depicted in Figure 5. The probability of the adsorption reaction is determined by the electrochemical potential of graphene (ζ_G) and that in the equilibrium condition of the oxygen-chemisorption reaction (ζ_{ads}). When

$\Delta G = \zeta_{ads} - \zeta_G < 0$, the electrons favorably transfer from graphene to the adsorbed oxygen (denoted by “A” in Figure 5a), and the oxygen-adsorption reaction proceeds. For charge transfer, the electrons should go through some energy barrier; we assume that electrons tunnel from BLG to the O_2 molecules via a *single* transition state (denoted by “T”), whose electrochemical potential is ζ_{TS} . The difference $\ddagger E = \zeta_{TS} - \zeta_G$ corresponds to the activation energy of the oxygen-chemisorption reaction, which determines the frequency of the electron transfer. Whereas ζ_G is dependent on the Fermi level ε_F as $\zeta_G = \varepsilon_F + \zeta_{CNP}$ (ζ_{CNP} is the electrochemical potential of the CNP), we envisage that ζ_{TS} (or $\ddagger E$) is a function of ε_F as well. In the framework of the Butler–Volmer theory, we obtain the dependence of $\ddagger E$ on ε_F as

$$\ddagger E(\varepsilon_F + d\varepsilon_F) = \ddagger E(\varepsilon_F) - \alpha d\varepsilon_F, \quad (2)$$

where $\alpha (> 0)$ is a constant related to the “transfer coefficient” in the Butler–Volmer theory that associates the activation energy with the *electrochemical potential* (not the Fermi energy); thus herein we call α as “pseudo transfer coefficient” (see Supporting Information for detail in the derivation). That is, we have the assumption that the activation energy scales linearly with the Fermi energy. Further assuming that the molecular adsorption rate dN_{ox}/dt is controlled by the electron transfer process and is not strongly affected by other contributions such as molecular diffusion¹⁴, it is given by

$$\frac{dN_{ox}}{dt} = \chi D(\varepsilon_F + \ddagger E(\varepsilon_F)) f(\varepsilon_F + \ddagger E(\varepsilon_F); \varepsilon_F), \quad (3)$$

where $D(\varepsilon)$ is the density of states (DOS) of BLG (ε is the energy measured from ζ_{CNP}) and $f(\varepsilon; \varepsilon_F) = [1 + (\varepsilon - \varepsilon_F)/k_B T]^{-1}$ is the Fermi–Dirac distribution function. The coefficient χ does not depend on ε_F (if the distance between the adsorbing molecules and BLG varied depending on ε_F or $V_{g,ad}$, the tunneling frequency would be affected so that χ might be dependent on them as well; yet herein we ignore such effect for simplicity). The right-side of Eq. (3) represents the tunneling rate of the electron from the graphene to oxygen at the energy level of transition state, $\varepsilon = \varepsilon_F + \ddagger E(\varepsilon_F) = \zeta_{TS} - \zeta_{CNP}$. According to Eq. (2) and Eq. (3), the molecular adsorption rate is dependent on the Fermi level of graphene. Using them, we can explain both the temporal evolution of the doping rate and its dependence on the gate voltage $V_{g,ad}$.

Let us discuss the temporal change in the doping rate. The Fermi level of graphene is lowered with the increase of the adsorbed oxygen molecules, because the positive charge is induced on graphene by the charge Ze they possess. Recalling that $\bar{n}_{ox} = -ZN_{ox}$, the doping rate is given by $d\bar{n}_{ox}/dt$. Furthermore, since $\ddagger E \gg k_B T$ is fulfilled as shown later, we also approximate that $f(\varepsilon_F + \ddagger E(\varepsilon_F); \varepsilon_F) \simeq \exp(-\ddagger E(\varepsilon_F)/k_B T)$. Using the relation $d\bar{n}_{ox} = -D(\varepsilon_F)d\varepsilon_F$, we acquire a formula describing the temporal change of the Fermi level:

$$-D(\varepsilon_F(t)) \frac{d\varepsilon_F(t)}{dt} = \frac{pk_B T}{\alpha_{te}} D(\varepsilon_F(t) + \ddagger E(\varepsilon_F(t))) \exp\left(\alpha_{te} \frac{\varepsilon_F(t) - \varepsilon_F(0)}{k_B T}\right), \quad (4)$$

where $\varepsilon_F(t) = \varepsilon_F(t, V_{g,ad})$, expressing that the Fermi level is a function of the exposure time t and the gate voltage $V_{g,ad}$, and $\varepsilon_F(0) = \varepsilon_F(0, V_{g,ad})$, the Fermi level at $t = 0$. We have specifically defined two constants, the pseudo transfer coefficient α_{te} (the subscript “te” abbreviates “temporal evolution”) and

$$p = -\frac{\alpha_{te} Z \chi}{k_B T} \exp\left(-\frac{\ddagger E(\varepsilon_F(0))}{k_B T}\right) \quad (5)$$

The right side of Eq. (4) represents the product of the charge transfer frequency and the amount of charge per adsorbed molecule, whereas the left side does the resultant amount of the doped charge. Because BLG (or also single layer graphene) has the low DOS around the CNP compared to metal, the small amount of carrier doping results in the large shift in the Fermi level, which effectively controls the kinetics. Thus the adsorption kinetics is well described by Eq. (4), the equation focusing on the Fermi level. When we envisage that the BLG is approximately described by two-dimensional parabolic dispersion of the free electron, the DOS becomes constant as $D \equiv D_P = \gamma_{\perp} / \pi (\hbar v_F)^2$, where $v_F = (\sqrt{3}/2) \gamma_0 a / \hbar$ is the Fermi velocity in SLG, $a = 2.46 \text{ \AA}$ is the in-plane lattice constant, and $\gamma_0 = 3.16 \text{ eV}$ and $\gamma_{\perp} \approx 0.4 \text{ eV}$ ^{51,52} are the intrasheet and intersheet transfer integrals, respectively. In this case (hereafter labeled as P kinetics), Eq. (6) is readily integrated, giving

$$\overline{n_{ox}}(t) = -\{\varepsilon_F(t) - \varepsilon_F(0)\} D_P = \left(\frac{k_B T D_P}{\alpha_{te}}\right) \ln(1 + pt) \quad (6)$$

Note that Eq. (6) satisfies $d\overline{n_{ox}}/dt \propto \exp[-\alpha_{te} \overline{n_{ox}}(t) / k_B T D]$ and is equivalent to the integrated form of Elovich equation^{53,54}, the empirical equation that is widely applicable to chemisorptions onto semiconductors. When the hyperbolic DOS of BLG⁴¹ is reflected to Eq. (4), more accurate but more complicated expression of $\varepsilon_F(t)$ is acquired (denoted as H kinetics), given by

$$-\frac{\alpha_{te}}{k_B T} \exp\left(\alpha_{te} \frac{\varepsilon_F(0)}{k_B T}\right) S[\varepsilon_F(0), \varepsilon_F(t)] + pt = 0, \quad (7)$$

where $S[\varepsilon_F(0), \varepsilon_F(t)]$ is a function that depends on the DOS at the Fermi level and that at the transition state level (derived in the Supporting Information).

We performed curve fitting of the experimental results of $\overline{n_{ox}}(t)$ with Eq. (6) and Eq. (7) for P kinetics and H kinetics, respectively. The difference in $V_{g,ad}$ by runs is simulated by the dependence of $\varepsilon_F(0)$ on $V_{g,ad}$ first without considering the gap-opening effect^{55,56}, that is,

we calculate $\varepsilon_F(0)$ using the relation that the charge of $c_g(V_{g,ad} - V_{CNP}^0)$ doped on BLG by applying $V_{g,ad}$ is equal to $\int_0^{\varepsilon_F(0)} D(\varepsilon) d\varepsilon$. Irrespective of the kinetic models, All the theoretical curves are well fitted to the experimental results except those for run 4 in the range above 10^3 min. Eq. (4) is invalid in the first place in the long-time regime in which the adsorption rate is almost as low as the desorption rate, since the present treatment includes no contribution of desorption. The deviation is, however, contrary to the expectation; the desorption should suppress the evolution of the hole doping yet the enhanced doping was actually observed. Thus we suspect that it is due to long-time scale chemisorption of oxygen onto graphene which is ubiquitously observed in carbon materials^{57,58}. Note that the several volts of offsets are added in V_{shift} (corresponding to the doping density of $2 \times 10^{11} \text{ cm}^{-2}$) to improve the fitting in the time range of $t \leq 10^0$ min. This small offset corresponds to a fast reaction that finishes at the very initial stage of adsorption, e.g., due to the reactive chemisorption of O_2 to the defect or edge site of graphene^{59,60}.

Figure 6 shows the profiles of the fitting results. Practically, the fitting parameters are following two: α_{te} and p , but in order to derive the initial activation energy before the oxygen adsorption, $\ddagger E(\varepsilon_F(0))$, from p based on Eq. (6), we briefly assume that the charge/molecular ratio is independent of the gate voltage and determine that $Z \chi \gamma_{\perp} = 1 \times 10^5 \text{ eV}^2 \text{ min}^{-1}$ from the pre-exponential factor in the literature³³, $c_{ox} \nu \kappa_{el} \sim 10^{17} \text{ cm}^{-2} \text{ s}^{-1}$ ($c_{ox} \nu \kappa_{el}$ in the literature corresponds to $\chi \gamma_{\perp} / \pi (\hbar v_F)^2$ in this paper). Note that if we assume another value than $Z \chi \gamma_{\perp} = 1 \times 10^5 \text{ eV}^2 \text{ min}^{-1}$, it results in a uniform shift of the calculated $\ddagger E(\varepsilon_F(0))$. In addition, the charge/molecular ratio of the adsorbed molecule Z is likely dependent on $V_{g,ad}$ from the discussion about the mobility, but it leads the shift of $\ddagger E(\varepsilon_F(0))$ only by $\sim k_B T = 0.026 \text{ eV}$. On the one hand, α_{te} (representing the temporal change of the activation energy) exhibits a significant deviation between the H kinetics and the P kinetics (Figure 6a), or depends on the treatment of the DOS of BLG. This deviation is understood as follows: H kinetics reflects the DOS of BLG that is a monotonically increasing function with respect to $|\varepsilon_F|$ having a minimum ($D = D_P$) at the CNP (Figure 6(c)), yet P kinetics does not. Since the downward shift of the Fermi level upon the oxygen adsorption depends on the DOS at the Fermi level, the range of the change in the Fermi level differs between two kinetics models (Figure 6(c)). Thus α_{te} , related with the Fermi level by Eq. (2), is calculated differently. This result is contrasted with the conventional electrochemical reaction on the metal electrodes in which the kinetics is not signif-

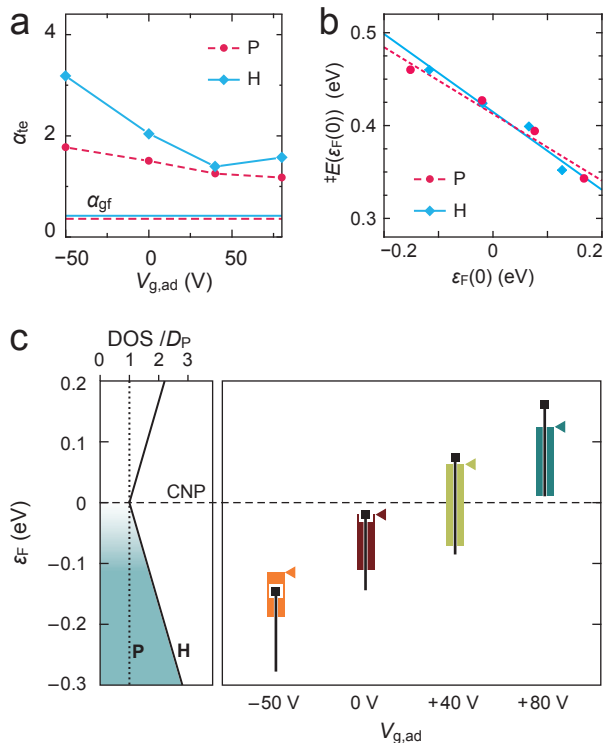


FIG. 6: Summary of parameters obtained by the curve fitting in Figure 2 with P kinetics (P) and H kinetics (H) compared. (a) Dependence of the pseudo transfer coefficient α_{te} on $V_{g,ad}$. The pseudo transfer coefficient α_{gf} acquired by the linear fitting to panel b is also plotted. (b) Initial activation energy $\ddagger E(\varepsilon_F(0))$ plotted as a function of $\varepsilon_F(0) = \varepsilon_F(0, V_g)$. (c) (Left panel) Density of states (DOS, solid line) for BLG as a function of the Fermi energy, where D_P (DOS at the energy of $\varepsilon_F = 0$) is taken as unit of the DOS. The solid line denotes the DOS applied for the H kinetics. In P kinetics the DOS is treated as constant; $D = D_P$ (dotted line). (Right panel) Change of the Fermi level by oxygen adsorption as a function of $V_{g,ad}$. Bars and boxes represent the range calculated under P kinetics and H kinetics, respectively, assuming $\gamma_{\perp} = 0.4$ eV. The Fermi level before the oxygen adsorption ($\varepsilon_F(0)$) is at the point indicated by triangles (black squares) for H (P) kinetics, whereas the Fermi level shifts downward with the increase of the adsorbed oxygen, and eventually reaches the bottom end of the boxes (bars) in the end of the oxygen adsorption for the H (P) kinetics. The energy is measured from the CNP (dashed line), and the gap-opening effect is not considered.

icantly affected by the DOS of the electrodes and is just owing to the low DOS of the BLG with comparison to the metal. On the other hand, we found that $\ddagger E(\varepsilon_F(0))$ is a decreasing function of $\varepsilon_F(0) = \varepsilon_F(0, V_{g,ad})$ (shown in Figure 6b, therein we plot $\ddagger E(\varepsilon_F(0))$ with respect to $\varepsilon_F(0)$ instead of $V_{g,ad}$). From Eq. (2), the slope of the plots in Figure 6b corresponds to the pseudo transfer coefficient α , and we found that $\alpha_{gf} = 0.36$ and 0.42 for P kinetics and H kinetics, respectively (the subscript “gf” abbreviates “gate electric field”). Herein we distinguish α_{gf} from α_{te} ; being different from α_{te} that is calculated based on

the temporal Fermi level shift by oxygen adsorption (thus α_{te} inevitably includes the oxygen adsorption effect), α_{gf} is acquired by tuning the Fermi level *electrically* at $t = 0$ before oxygen adsorption. We found that α_{gf} is much smaller than $\alpha_{te} (\geq 1)$, or rather near 0.5, a typical transfer coefficient for simple redox reactions^{48,49} (Figure 6a). Specifically, the oxygen adsorption effect included only in α_{te} but not in α_{gf} is attributed, e.g., to the electric dipole layer⁶¹ formed between graphene and the adsorbed molecules and the Coulomb interaction between the adsorbed oxygen molecules. We expect that these effects also raise the activation energy roughly in proportional to the number of molecules N_{ox} (or the doping density $\overline{n_{ox}}$), and thus we have the expression for the additional adsorption effect: $d\ddagger E = \xi_{mol} d\overline{n_{ox}} = -\xi_{mol} D(\varepsilon_F) d\varepsilon_F$ (ξ_{mol} : the proportional coefficient; herein we use the relation $d\overline{n_{ox}} = -D(\varepsilon_F) d\varepsilon_F$ again). Then we acquire $\alpha_{te} \simeq \alpha_{gf} + \xi_{mol} \langle D(\varepsilon_F) \rangle$ ($\langle D(\varepsilon_F) \rangle$ denotes the average DOS in the range of the Fermi level for each run), which indicates that α_{te} is large when the DOS is large in the level far away from the CNP (see Figure 6c). Indeed, as shown in Figure 6a, α_{te} for H kinetics shows the V-shaped dependence on $V_{g,ad}$ with the minimum for $V_{g,ad} = +40$ V, which gives the smallest average DOS. Though the kinetics for the molecular adsorption is affected by various effects as mentioned above, we represent them by the parameter α_{te} and succeed in accounting for the observed kinetics in a facile way.

Finally let us account for the power-law dependence of $d\overline{n_{ox}}/dt \propto t^{-u}$ shown in Figure 3. It is helpful to look on the simpler P kinetics for the assessment of $d\overline{n_{ox}}/dt$; from Eq. (6), we obtain $d\overline{n_{ox}}/dt \propto p/(1+pt)$. Approximately we have $d\overline{n_{ox}}/dt \propto (u\langle t \rangle^{u-1}) t^{-u}$ where $u \simeq [1 + (1/p\langle t \rangle)]^{-1} \leq 1$ (the time $\langle t \rangle$ is the center of the expansion of $\ln(d\overline{n_{ox}}/dt)$ in terms of $\ln t$, and it is a good approximation if $p\langle t \rangle \gg 1$, or otherwise if $p\langle t \rangle \simeq 1$ in the time range such that $t = [10^{-1}\langle t \rangle, 10\langle t \rangle]$). Since p is intensively dependent on $V_{g,ad}$ (recall that (i) p is exponentially decaying against $\ddagger E(\varepsilon_F(0))$ as represented in Eq. (5), (ii) $\ddagger E(\varepsilon_F(0))$ linearly decreases with respect to $\varepsilon_F(0)$ with the slope of $-\alpha_{gf}$ as shown in Figure 6c, (iii) $\varepsilon_F(0)$ is an increasing function of $V_{g,ad}$. We acquired $p = 19.6, 2.9, 0.98$ and 0.32 for $V_{g,ad} = +80, +40, 0$, and -50 V, respectively, by fitting within the P kinetics model), we can find that u is almost unity for a positively high $V_{g,ad}$ and tends to be smaller for negatively high $V_{g,ad}$ within the time range experimentally scoped, which is consistent with the observed behavior. When the electrochemical mechanism governs the kinetics of the oxygen adsorption, the activation energy of the charge transfer continually increases with the O_2 exposure time increasing. This effect leads to non-Langmurian kinetics of the oxygen adsorption and the power-law decrease of $d\overline{n_{ox}}/dt$, even though neither the desorption process nor the saturation limit of adsorption are taken into consideration.

In BLG, it is known that a band gap opens due to the energy difference between two layers⁹. The gate electric

field as well as the adsorbed oxygen may produce such a strong energy difference that the eventual band gap should affect the time evolution of molecular adsorption. The band gap opening effect is expected to exhibit most prominently when the Fermi level goes across the CNP (at the point shown by arrows in Figure 2), while we cannot find such behavior obviously. We guess it is partly because most of the adsorbed oxygen molecules exist in the interface between graphene and the gate dielectric SiO₂. For the band gap opening effect to appear, it is necessary that the gate electric field and the molecular field enhance each other when the Fermi level is near the CNP (i.e., the charge induced by the gate electric field and that by the adsorbed molecules including unintentional residual impurities on the SiO₂ substrate are balanced), yet it is possible only when the molecules mainly adsorb on the top surface of BLG, and not for the molecules adsorbed in the interface (Figure S2, Supporting Information). Or it may be partly because the disordered potential due to the impurities in the substrate fluctuates the energy level around which the band gap exists⁶², eventually blurring band gap opening effects and chemical reactivity⁶³ of BLG. Details about the band-gap opening effects are discussed in the Supporting Information.

In summary, we investigated the weak chemisorption of O₂ molecules on bilayer graphene by measuring its transport properties. The hole doping due to O₂ chemisorption is remarkably dependent on the gate voltage, and the amount of the doped carrier increases with O₂ exposure time, the rate of which is in accordance with $\propto t^{-u}$ ($u \leq 1$) rather than with conventional Langmuirian kinetics. We conclude from these that an electrochem-

ical reaction governs the O₂ chemisorption process, in which the rate of the chemisorption is determined by the Fermi level of graphene, and indeed succeed in accounting for the observed kinetics by the analysis based on the Butler–Volmer theory. We also found that the chemisorbed molecules decrease the mobility of graphene, and interestingly, the mobility change is dependent on the gate voltage applied during the adsorption, indicating that the adsorption state, e.g., transferred charge or distance between a molecule and graphene, can be modified electrically. Graphene, offering a continuously tunable platform for study of chemisorptions on it, realizes the electrical control of the adsorption by gate electric field, a novel and versatile method in which we would explore extensively a wider variety of host–guest interactions between graphene and foreign molecules.

Supporting Information. Additional descriptions about (i) the experimental method, (ii) the electrochemistry-based kinetics model and the mathematical derivation for it, and (iii) an expanded discussion about the gap-opening effects.

Acknowledgments

The authors acknowledge support from Grant-in-Aid for Scientific Research No. 20001006 from the Ministry of Education, Culture, Sports, Science and Technology, Japan. The authors thank M. Kiguchi, T. Kawakami, K. Yokota, and Y. Kudo for useful discussion.

* Electronic address: [mail to: sato.y.an@m.titech.ac.jp](mailto:sato.y.an@m.titech.ac.jp)

¹ R. Balog, B. Jørgensen, L. Nilsson, M. Andersen, E. Rienks, M. Bianchi, M. Fanetti, E. Laegsgaard, A. Baraldi, S. Lizzit, Z. Sljivancanin, F. Besenbacher, B. Hammer, T. G. Pedersen, P. Hofmann, and L. Hornekær, *Nat. Mater.* **9**, 315 (2010).
² Y. Zhang, A. Kolmakov, S. Chretien, H. Metiu, and M. Moskovits, *Nano Lett.* **4**, 403 (2004).
³ A. H. Castro Neto, F. Guinea, N. M. R. Peres, K. S. Novoselov, and A. K. Geim, *Rev. Mod. Phys.* **81**, 109 (2009).
⁴ F. Schedin, A. K. Geim, S. V. Morozov, E. W. Hill, P. Blake, M. I. Katsnelson, and K. S. Novoselov, *Nat. Mater.* **6**, 652 (2007).
⁵ J. H. Chen, C. Jang, S. Adam, M. S. Fuhrer, E. D. Williams, and M. Ishigami, *Nat. Phys.* **4**, 377 (2008).
⁶ S. Xiao, J.-H. Chen, S. Adam, E. D. Williams, and M. S. Fuhrer, *Phys. Rev. B* **82**, 041406 (2010).
⁷ J. H. Chen, C. Jang, M. Ishigami, S. Xiao, W. G. Cullen, E. D. Williams, and M. S. Fuhrer, *Sol. Stat. Commun.* **149**, 1080 (2009).
⁸ D. W. Boukhalov and M. I. Katsnelson, *Appl. Phys. Lett.* **95**, 023109 (2009).
⁹ E. V. Castro, K. S. Novoselov, S. V. Morozov,

N. M. R. Peres, J. M. B. Lopes dos Santos, J. Nilsson, F. Guinea, A. K. Geim, and A. H. Castro Neto, *J. Phys.: Condens. Matter* **22**, 175503 (2010).
¹⁰ D. A. Abanin, A. V. Shytov, and L. S. Levitov, *Phys. Rev. Lett.* **105**, 086802 (2010).
¹¹ R. M. Ribeiro, N. M. R. Peres, J. Coutinho, and P. R. Briddon, *Phys. Rev. B* **78**, 075442 (2008).
¹² T. Lohmann, K. von Klitzing, and J. H. Smet, *Nano Lett.* **9**, 1973 (2009).
¹³ V. V. Cheianov, O. Syljuåsen, B. L. Altshuler, and V. I. Fal’ko, *EPL* **89**, 56003 (2010).
¹⁴ H. E. Romero, P. Joshi, A. K. Gupta, H. R. Gutierrez, M. W. Cole, S. A. Tadigadapa, and P. C. Eklund, *Nanotechnology* **20**, 245501 (2009).
¹⁵ T. O. Wehling, M. I. Katsnelson, and A. I. Lichtenstein, *Chem. Phys. Lett.* **476**, 125 (2009).
¹⁶ K. Takai, S. Eto, M. Inaguma, T. Enoki, H. Ogata, M. Tokita, and J. Watanabe, *Phys. Rev. Lett.* **98**, 017203 (2007).
¹⁷ K. M. McCreary, K. Pi, A. G. Swartz, W. Han, W. Bao, C. N. Lau, F. Guinea, M. I. Katsnelson, and R. K. Kawakami, *Phys. Rev. B* **81**, 115453 (2010).
¹⁸ K. S. Novoselov, A. K. Geim, S. V. Morozov, D. Jiang, M. I. Katsnelson, I. V. Grigorieva, S. V. Dubonos, and

- A. A. Firsov, *Nature* **438**, 197 (2005).
- ¹⁹ J. Zhou, Q. Wang, Q. Sun, P. Jena, and X. S. Chen, *Proc. Natl. Acad. Sci. USA* **107**, 2801 (2010).
- ²⁰ P. Saalfrank, *J. Chem. Phys.* **113**, 3780 (2000).
- ²¹ W. Liu, Y. H. Zhao, J. Nguyen, Y. Li, Q. Jiang, and E. J. Lavernia, *Carbon* **47**, 3452 (2009).
- ²² Y.-H. Lu, L. Shi, C. Zhang, and Y.-P. Feng, *Phys. Rev. B* **80**, 233410 (2009).
- ²³ V. W. Brar, R. Decker, H.-M. Solowan, Y. Wang, L. Maserati, K. T. Chan, H. Lee, c. O. Girit, A. Zettl, S. G. Louie, M. L. Cohen, and M. F. Crommie, *Nat. Phys.* **7**, 43 (2011).
- ²⁴ J.-H. Parq, J. Yu, Y.-K. Kwon, and G. Kim, *Phys. Rev. B* **82**, 193406 (2010).
- ²⁵ X. Tian, J. Xu, and X. Wang, *J. Phys. Chem. B* **114**, 11377 (2010).
- ²⁶ A. M. Suarez, L. R. Radovic, E. Bar-Ziv, and J. O. Sofo, *Phys. Rev. Lett.* **106**, 146802 (2011).
- ²⁷ A. A. Kaverzin, S. M. Strawbridge, A. S. Price, F. Withers, A. K. Savchenko, and D. W. Horsell, *Carbon* **49**, 3829 (2011).
- ²⁸ H. Pinto, R. Jones, J. P. Goss, and P. R. Briddon, *Phys. Status Solidi. A* **207**, 2131 (2010).
- ²⁹ Y. Yang and R. Murali, *Appl. Phys. Lett.* **98**, 093116 (2011).
- ³⁰ P. L. de Andres and J. A. Vergés, *Appl. Phys. Lett.* **93**, 171915 (2008).
- ³¹ Y. Shi, W. Fang, K. Zhang, W. Zhang, and L.-J. Li, *Small* **5**, 2005 (2009).
- ³² C. M. Aguirre, P. L. Levesque, M. Paillet, F. Lapointe, B. C. St-Antoine, P. Desjardins, and R. Martel, *Adv. Mater.* **21**, 3087 (2009).
- ³³ P. L. Levesque, S. S. Sabri, C. M. Aguirre, J. Guillemette, M. Sijaj, P. Desjardins, T. Szkopek, and R. Martel, *Nano Lett.* **11**, 132 (2010).
- ³⁴ S. S. Sabri, P. L. Lévesque, C. M. Aguirre, J. Guillemette, R. Martel, and T. Szkopek, *Appl. Phys. Lett.* **95**, 242104 (2009).
- ³⁵ R. Nouchi and K. Tanigaki, *Appl. Phys. Lett.* **96**, 253503 (2010).
- ³⁶ T. Yamada, *Phys. Rev. B* **69**, 125408 (2004).
- ³⁷ S. Das Sarma, S. Adam, E. H. Hwang, and E. Rossi, *Rev. Mod. Phys.* **83**, 407 (2011).
- ³⁸ S. Adam and S. Das Sarma, *Phys. Rev. B* **77**, 115436 (2008).
- ³⁹ M. Monteverde, C. Ojeda-Aristizabal, R. Weil, K. Bennaceur, M. Ferrier, S. Guéron, C. Glatli, H. Bouchiat, J. N. Fuchs, and D. L. Maslov, *Phys. Rev. Lett.* **104**, 126801 (2010), Supplementary Material II.
- ⁴⁰ E. McCann and V. I. Fal'ko, *Phys. Rev. Lett.* **96**, 086805 (2006).
- ⁴¹ S. Adam and M. D. Stiles, *Phys. Rev. B* **82**, 075423 (2010).
- ⁴² S. Adam, E. H. Hwang, V. M. Galitski, and S. Das Sarma, *Proc. Natl. Acad. Sci. USA* **104**, 18392 (2007).
- ⁴³ Y. W. Tan, Y. Zhang, K. Bolotin, Y. Zhao, S. Adam, E. H. Hwang, S. Das Sarma, H. L. Stormer, and P. Kim, *Phys. Rev. Lett.* **99**, 246803 (2007).
- ⁴⁴ K. M. Ervin, I. Anusiewicz, P. Skurski, J. Simons, and W. C. Lineberger, *J. Phys. Chem. A* **107**, 8521 (2003).
- ⁴⁵ S. J. Sque, R. Jones, and P. R. Briddon, *Phys. Status Solidi A* **204**, 3078 (2007).
- ⁴⁶ V. Chakrapani, J. C. Angus, A. B. Anderson, S. D. Wolter, B. R. Stoner, and G. U. Sumanasekera, *Science* **318**, 1424 (2007).
- ⁴⁷ S. Ryu, L. Liu, S. Berciaud, Y.-J. Yu, H. Liu, P. Kim, G. W. Flynn, and L. E. Brus, *Nano Lett.* **10**, 4944 (2010).
- ⁴⁸ I. Heller, J. Kong, K. A. Williams, C. Dekker, and S. G. Lemay, *J. Am. Chem. Soc.* **128**, 7353 (2006).
- ⁴⁹ J. O. M. Bockris and Z. Nagy, *J. Chem. Educ.* **50**, 839 (1973).
- ⁵⁰ J. O. Bockris, A. K. N. Reddy, and M. Gamboa-Aldeco, *Fundamentals of Electrodicts*, 2nd ed., Modern Electrochemistry, Vol. 2A (Plenum Press, 2000).
- ⁵¹ W. W. Toy, M. S. Dresselhaus, and G. Dresselhaus, *Phys. Rev. B* **15**, 4077 (1977).
- ⁵² M. S. Dresselhaus and G. Dresselhaus, *Adv. Phys.* **51**, 1 (2002).
- ⁵³ C. Aharoni and F. C. Tompkins, *Kinetics of adsorption and desorption and the Elovich equation*, edited by D. D. Eley, H. Pines, and P. B. Weisz, Vol. 21 (Academic Press, New York and London, 1970) pp. 1–49.
- ⁵⁴ I. S. McIntock, *Nature* **216**, 1204 (1967).
- ⁵⁵ T. Ohta, A. Bostwick, T. Seyller, K. Horn, and E. Rotenberg, *Science* **313**, 951 (2006).
- ⁵⁶ E. V. Castro, K. S. Novoselov, S. V. Morozov, N. M. R. Peres, J. M. B. L. dos Santos, J. Nilsson, F. Guinea, A. K. Geim, and A. H. Castro Neto, *Phys. Rev. Lett.* **99**, 216802 (2007).
- ⁵⁷ N. Kobayashi, T. Enoki, C. Ishii, K. Kaneko, and M. Endo, *J. Chem. Phys.* **109**, 1983 (1998).
- ⁵⁸ G. U. Sumanasekera, G. Chen, K. Takai, J. Joly, N. Kobayashi, T. Enoki, and P. C. Eklund, *J. Phys. Condens. Matter* **22**, 334208 (2010).
- ⁵⁹ X. Wang and H. Dai, *Nat. Chem.* **2**, 661 (2010).
- ⁶⁰ F. M. Koehler, A. Jacobsen, K. Ensslin, C. Stampfer, and W. J. Stark, *Small* **6**, 1125 (2010).
- ⁶¹ G. Giovannetti, P. A. Khomyakov, G. Brocks, V. M. Karpan, J. van den Brink, and P. J. Kelly, *Phys. Rev. Lett.* **101**, 026803 (2008).
- ⁶² G. M. Rutter, S. Jung, N. N. Klimov, D. B. Newell, N. B. Zhitenev, and J. A. Stroscio, *Nat. Phys.* **7**, 649 (2011).
- ⁶³ R. Sharma, J. H. Baik, C. J. Perera, and M. S. Strano, *Nano Lett.* **10**, 398 (2010).